
Mol-PECO: a deep learning model to predict human olfactory perception from molecular structures

Mengji Zhang*

School of Biomedical Engineering, Shanghai Jiao Tong University, Shanghai, 200030, China
Institute of Industrial Science, The University of Tokyo, Meguro-ku, Tokyo, 153-8505, Japan
mengji.zhang0809@gmail.com

Yusuke Hiki

Department of Biosciences and Informatics
Keio University
Kouhoku-ku, Yokohama, 223-8522, Japan
hiki@fun.bio.keio.ac.jp

Akira Funahashi

Department of Biosciences and Informatics
Keio University
Kouhoku-ku, Yokohama, 223-8522, Japan
funa@bio.keio.ac.jp

Tetsuya J. Kobayashi†

Institute of Industrial Science
The University of Tokyo
Meguro-ku, Tokyo, 153-8505, Japan
tetsuya@mail.crmind.net

Abstract

While visual and auditory information conveyed by wavelength of light and frequency of sound have been decoded, predicting olfactory information encoded by the combination of odorants remains challenging due to the unknown and potentially discontinuous perceptual space of smells and odorants. Herein, we develop a deep learning model called Mol-PECO (**M**olecular Representation by **P**ositional **E**ncoding of **C**oulomb Matrix) to predict olfactory perception from molecular structures. Mol-PECO updates the learned atom embedding by directional graph convolutional networks (GCN), which model the Laplacian eigenfunctions as positional encoding, and Coulomb matrix, which encodes atomic coordinates and charges. With a comprehensive dataset of 8,503 molecules, Mol-PECO directly achieves an area-under-the-receiver-operating-characteristic (AUROC) of 0.813 in 118 odor descriptors, superior to the machine learning of molecular fingerprints (AUROC of 0.761) and GCN of adjacency matrix (AUROC of 0.678). The learned embeddings by Mol-PECO also capture a meaningful odor space with global clustering of descriptors and local retrieval of similar odorants. Our work may promote the understanding and decoding of the olfactory sense and mechanisms.

1 Introduction

Olfaction is one of the essential senses, where the sense of smell is triggered by the binding of odorant molecules to olfactory receptors and is shaped by the subsequent neural processing of the received information in the brain[Sobel et al., 1998, Lapid et al., 2011]. Unlike vision and hearing, however, the prediction of olfactory perception for odorant molecules remains challenging. On the one hand, some

*This work is done as a visiting student in Tokyo University.

†Correspondence to Tetsuya J. Kobayashi or Mengji Zhang.

molecules with different functional groups share identical smells[Sell, 2006]. On the other hand, other molecules with similar structures can produce totally different perceptions[Boesveldt et al., 2010]. The structures and perceptions of the odorant molecules are nonlinearly and discontinuously related[Keller et al., 2017]. Unveiling the quantitative structure-odor relationship (QSOR) is indispensable for understanding the coding principle of olfactory information[Keller et al., 2017] and also essential for predicting and designing smells and flavors for various applications such as food technologies[Polster and Schieberle, 2017].

Machine learning (ML) is a promising approach to untangle such a complicated relationship. However, the prediction of olfactory perception from molecular structures is strongly dependent on molecular representation[Pattanaik and Coley, 2020]. Molecular fingerprints, which encode chemical substructures into fixed-length vectors, are the major and classical molecular representation, yet demonstrate limited performances in QSOR due to the inefficient feature extraction by hand-crafted rules[Rogers and Hahn, 2010, Moriwaki et al., 2018]. To learn a good representation of molecules from data, graph convolutional networks (GCNs) have been widely applied in molecular modeling[Kipf and Welling, 2016], e.g., quantum chemistry[Hofstetter et al., 2022, Yang et al., 2019, Feinberg et al., 2018], biophysics[Wang et al., 2019, Withnall et al., 2020], and biological side effects[Yang et al., 2019, Withnall et al., 2020]. The conventional GCN models each molecule by the adjacency matrix, which encodes the chemical bonds as a graph, and performs the information aggregation among the neighbors prescribed by the adjacency matrix[Yang et al., 2019, Sanchez-Lengeling et al., 2019]. While GCN has been reported to outperform conventional ML with molecular fingerprints in standard tasks[Sanchez-Lengeling et al., 2019], it still has technical drawbacks, which potentially limit the applicability of GCN and the adjacency matrix ([Kreuzer et al., 2021, Oono and Suzuki, 2019, Topping et al., 2021]) to learning QSOR. First, the adjacency matrix cannot encode the atomic and global 3D information of molecules[Pattanaik and Coley, 2020], even though such atomic and 3D information is the major determinant of binding affinities between odorant molecules and olfactory receptors[Floriano et al., 2000]. Second, graphs do not have a canonical coordinate representation, which contrasts with sequences and images for which one-, two-, and three-dimensional lattice coordinates are canonical. As a result, the GCN employs permutation invariant operations, e.g., message passing or neighboring aggregation, which then limit its expressive power to discriminate molecules with different structures([Kreuzer et al., 2021]) and also induces oversmoothing[Oono and Suzuki, 2019] and oversquashing[Topping et al., 2021]. All of these factors may hamper the network to efficiently learn the QSOR of odorant molecules with a variety of structures.

In this work, we develop a deep learning model (Mol-PECO) for QSOR, which aims at the multi-label classification of olfactory perception from molecular structure (Figure 1). To address the problems in conventional ML and GCN approaches, Mol-PECO combines the Coulomb matrix (CM) and Spectral Attention Network (SAN). CM is a simple global representation of a molecule by Coulombic forces between atoms in the molecule calculated with the nuclear charges and the corresponding 3D coordinates[Rupp et al., 2012]. CM therefore could encode more detailed structural information than the adjacency matrix which only represents the chemical bonds between atoms. SAN is an architecture of graph attention network (GAT)[Kreuzer et al., 2021], which uses the full Laplacian spectrum of a molecular graph for a learned positional encoding (LPE). Eigenfunctions of the graph Laplacian hierarchically describe the global and local structures in a graph and thereby provides a way to canonically characterize graphs and to define positional information of nodes (atoms)[Dwivedi and Bresson, 2020]. SAN can also be categorized as an attempt to extend the expressive power in graph-based architectures by endowing a canonical coordinate or positional information with graphs by using their spectral information[Beaini et al., 2021, Kreuzer et al., 2021, Dwivedi and Bresson, 2020]. CM can be naturally combined with SAT by regarding CM as a weighted adjacency matrix.

Based on the learned representation, Mol-PECO directly predicts 118 odor descriptors of perception for each odorant molecule. Mol-PECO achieves area under the receiver operating characteristic curve (AUROC) of 0.813 and area under the precision-recall curve (AUPRC) of 0.181, whereas the conventional MLs of molecular fingerprints fail to balance AUROC and AUPRC; the ML method (cfps-KNN) with the highest AUROC of 0.761 has low AUPRC of 0.057 and one (mordreds-RF) with the highest AUPRC of 0.144 shows low AUROC of 0.723. Thus, Mol-PECO may boost the prediction of QSOR for applications and also contribute to the understanding of the principle underlying olfactory information processing.

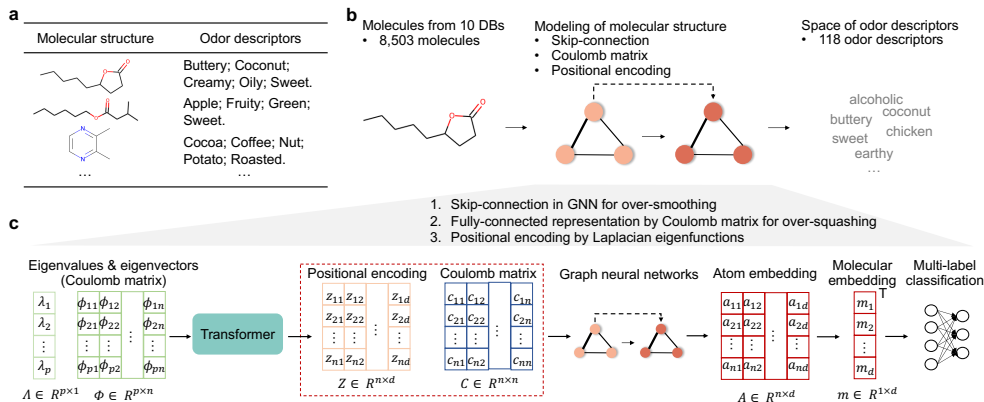


Figure 1: Overview of Mol-PECO. (a) Typical molecular structures and the corresponding odor descriptors are shown as examples. (b) The main workflow of modeling quantitative structure-odor relationship (QSOR). (c) The detailed model architecture of Mol-PECO and its three features: 1) skip-connection in graph neural networks to alleviate over-smoothing, 2) fully-connected molecular representation by Coulomb matrix to suppress over-squashing, and 3) positional encoding by Laplacian eigenfunctions.

2 Dataset: A comprehensive human olfactory perception dataset

In this work, we use the data in which each molecular structure is paired with multiple odor descriptors (Figure 1 a). The dataset in our work is compiled from ten expert-labeled sources: Arctander’s dataset ($n = 3,102$, [Arctander et al., 1960]), AromaDb ($n = 1,194$, [Kumar et al., 2018]), FlavorDb ($n = 525$, [Garg et al., 2018]), FlavorNet ($n = 718$, [Acree, 2004]), Goodscents ($n = 6,158$, [Flavor]), Fragrance Ingredient Glossary ($n = 1,135$, [Association et al., 2003]), Leffingwell’s dataset ($n = 3,523$, [Leffingwell, 2001]), Sharma’s dataset ($n = 4,006$, [Sharma et al., 2021]), OlfactionBase ($n = 5,105$, [Sharma et al., 2022]), and Sigma’s Fragrance and Flavor Catalog ($n = 871$, [Corporation, 2011]). These datasets are retrieved from the archive of <https://github.com/pyrfume/pyrfume-data>. The data cleaning procedure includes 1) merging the overlapped molecules, 2) filtering the conflict descriptors, and 3) filtering the rare descriptors assigned to less than 30 molecules. After data cleaning, we obtain a comprehensive dataset of 8,503 molecules and 118 odor descriptors.

This comprehensive human olfactory perception dataset is multi-labeled, with every molecule labeled with one or several odor descriptors. For the number of molecules associated with each odor descriptor, the distribution is imbalanced: each of 112 odor descriptors possesses ≤ 800 molecules whereas the other 6 descriptors possess > 800 molecules (Figure 2 a). For the number of descriptors associated with each molecule, the distribution is also skewed, with 8,054 molecules possessing ≤ 5 odor descriptors and 449 molecules possessing > 5 odor descriptors (Figure 2 b). For co-occurrence, descriptors of ‘fruity’, ‘green’, ‘sweet’, ‘floral’, and ‘woody’ co-occur with almost all the descriptors, while odorless molecules co-occur with no other molecules (Figure 2 c). The data split is built by second-order iterative stratification [Szymański and Kajdanowicz, 2017], which aims at splitting multi-label dataset and preserves the label ratios in each split with an iterative sampling design. The whole dataset is splitted into train / validation / test datasets of 6,802 / 864 / 837 pairs, respectively.

3 Results

In this section, we first introduce Coulomb-GCN, which updates GCN by replacing the adjacency matrix with CM. After verifying the effectiveness of Coulomb-GCN, we have Mol-PECO by further replacing the random embedding of atoms in Coulomb-GCN with positional encoding, in which the spectral information of the CM is employed to have a structure-aware embedding.

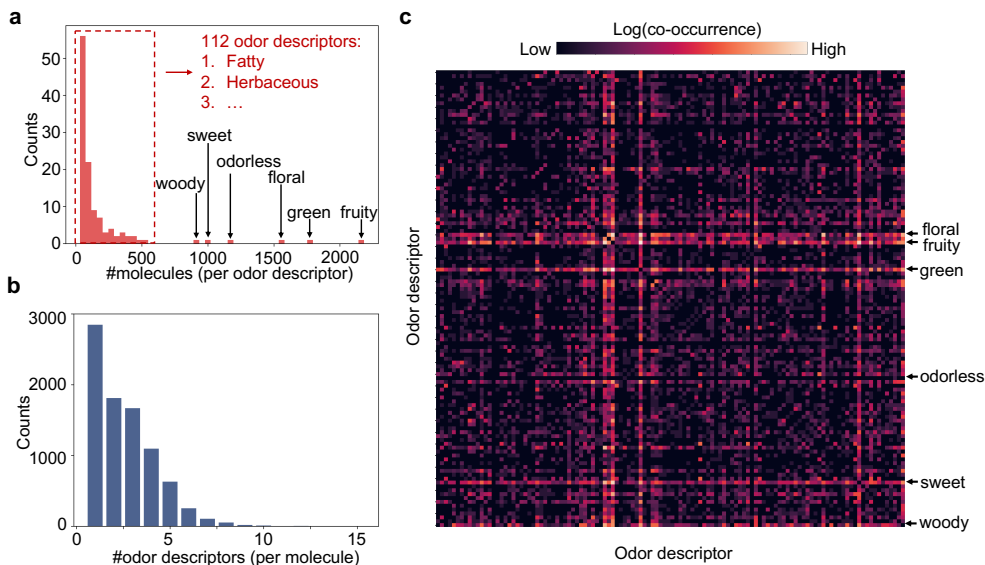


Figure 2: The comprehensive human olfactory dataset. (a) Distribution of molecules across odor descriptors. (b) Distribution of descriptors across molecules. (c) Co-occurrence matrix of 118 odor descriptors. The heatmap is demonstrated with logarithm transformation, and the descriptors are ordered alphabetically.

3.1 Fully-connected graph by Coulomb matrix is superior to sparse graph by adjacency matrix

We calculate CM, which models atomic energies with the internuclear Coulomb repulsion operator [Rupp et al., 2012, Schrier, 2020], and use it as our molecular representation. In CM, the diagonal entries refer to a polynomial fit of atomic energies and off-diagonal entries represent the Coulomb repulsion force between atomic nuclei. Although the adjacency matrix has been widely used in molecular modeling [Mahmood et al., 2021, Wang et al., 2022], CM as an emerging molecular representation can have at least two advantages: 1) CM handles the over-squashing plight by allowing direct paths between distant nodes in the fully-connected graph representation (Figure 3a); 2) distance by Frobenius norm between CM and adjacency matrix is 5–10 times smaller than that between random initialized matrix and adjacency matrix, indicating that CM is fully-connected while preserving a similarity to adjacency matrix (Figure 3b).

We build a nonlinear map (named Coulomb-GCN) between molecular structures and human olfactory perception (Figure 3c) by replacing the adjacency matrix in message passing of GCN with CM. Specifically, starting from random atom embedding, the learned atom embedding is obtained by message passing on fully-connected molecular graph with neighbor weights specified by the entries of CM. The molecular embedding is extracted by sum pooling and fed to a multi-label classification module to predict 118 odor descriptors. Considering the gap between maximal and minimal entries in CM, normalization of entries may affect the performance. We test Minmax and Frobenius normalizations in a matrix-wise manner.

We evaluate and compare the prediction accuracy of GCN with adjacency matrix and those of Coulomb-GCN with the different normalizations of CM (Table 1). Compared with GCN with adjacency matrix (AUROC of 0.678), gains in AUROC are observed in Coulomb-GCN with Frobenius normalization (AUROC of 0.759) and minmax normalization (AUROC of 0.713). Coulomb-GCN with Frobenius normalization also achieves higher performances in five out of six evaluation metrics (Table 1): AUROC (improved from 0.678 to 0.759), AUPRC (improved from 0.111 to 0.143), specificity (improved from 0.625 to 0.744), precision (improved from 0.079 to 0.089), and accuracy (improved from 0.726 to 0.780).

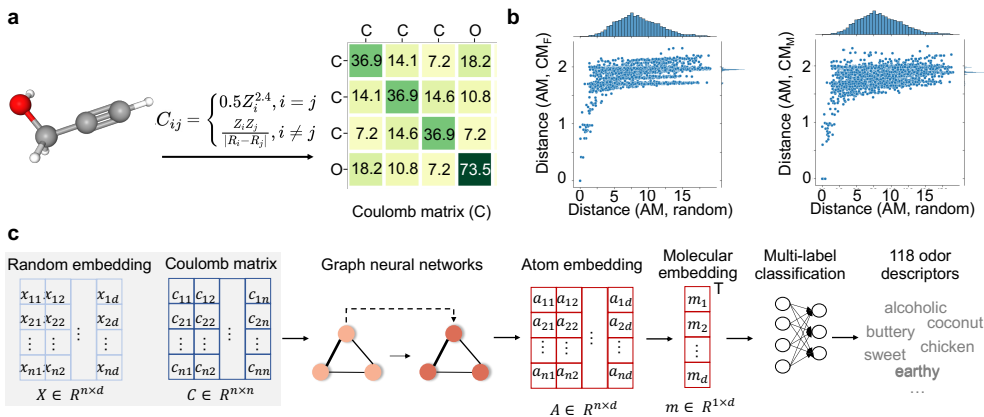


Figure 3: The motivation and workflow of modeling the Coulomb matrix. (a) An example of Coulomb matrix as a fully-connected graph for Propargyl alcohol, a clear colorless liquid with a geranium-like odor. (b) Similarity between Coulomb matrix and adjacency matrix, indicated by the distances. The distance is calculated with the Frobenius norm. (c) The workflow of modeling Coulomb matrix by graph neural networks.

Table 1: Prediction performances of Coulomb matrix with Minmax and Frobenius normalizations and adjacency matrix in GCN. The highest score of each metric is shown in bold.

Representation	Normalization ¹	AUROC	AUPRC	Precision	Recall	Specificity	Accuracy
Adjacency matrix	-	0.678	0.111	0.079	0.827	0.625	0.726
Coulomb matrix	Minmax	0.713	0.138	0.082	0.811	0.687	0.749
Coulomb matrix	Frobenius	0.759	0.143	0.089	0.816	0.744	0.780

¹ Normalization refers to the normalization methods for Coulomb matrix.

3.2 Directional graph modeling by Laplacian eigenfunctions improves prediction accuracy

The graph Laplacian and its spectral information enable us to characterize the global and substructures of graphs [Mohar et al., 1991, Chung, 1997, Spielman, 2012]. Specifically, the graph Laplacian is defined as $L = D - A$, where D and A refer to the degree and adjacency matrices. L is positive semi-definite with one trivial and the other nontrivial eigenvalues. In this work, the Laplacian defined by CM acts as an extension of the normal Laplacian ($L = D - W$), where W refers to the weighted matrix (CM in this work) and possesses the same properties as the graph Laplacian (e.g., symmetric and positive semi-definite). In particular, the eigenvectors of L provide an optimal solution to the Laplacian quadratic form ($f^T L f = 1/2 \sum_{i,j} X(i,j)(f_i - f_j)^2$) [Mohar et al., 1991, Spielman, 2012, Chung, 1997], encoding the geometric information of graphs.

Given these properties of the Laplacian graph, we use the Laplacian eigenfunctions of the CM to encode the positional information of molecular graphs. Typical results of a cyclic odorant (5-pentylloxolan-2-one, flowing from left to right in λ_1) and acyclic odorants (hexyl 3-methylbutanoate, flowing from left to right in λ_1 , and heptyl pentanoate, flowing from right to left in λ_1) demonstrate the information carried by low frequency eigenfunctions (Figure 4 a). Combining it with the Coulomb-GCN, we construct the deep learning framework, named Mol-PECO (Figure 4b), with the fully-connected molecular representation by CM and the positional encoding by Laplacian. We choose LPE by Transformer [Kreuzer et al., 2021] to build the atom embedding. Specifically, LPE concatenates the p lowest eigenvalues and the corresponding eigenvectors as the input matrix $\Lambda \in R^{p \times 2}$, and learns the encoding with Transformer for every atom [Kreuzer et al., 2021]. We obtain AUROC of 0.796 and AUPRC of 0.153 with LPE of raw CM. We further perform the experiments for LPE of asymmetric normalized CM and obtain additional gain of performances by 0.017 and 0.028 for AUROC and AUPRC, respectively.

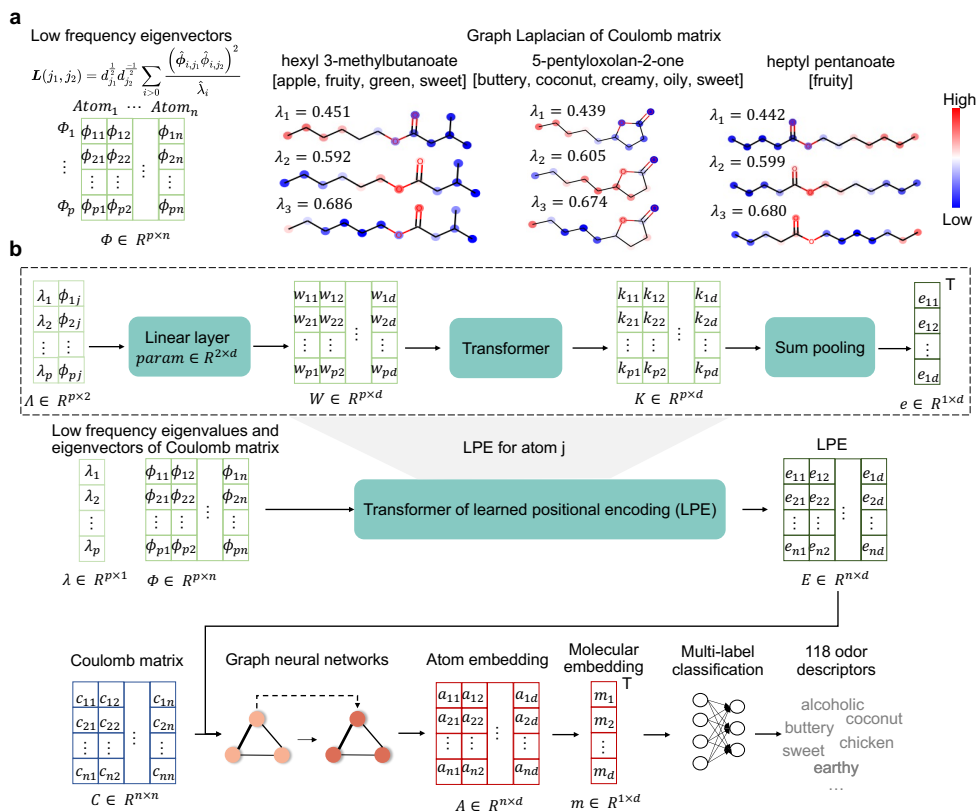


Figure 4: The motivation and architecture of Mol-PECO. (a) Structural information carried by the Laplace spectrum of the Coulomb matrix. Low-frequency eigenvectors, calculated with graph Laplacian, as the input matrix for positional encoding and 3 examples, including cyclic and acyclic molecules, of eigenvalue λ_i and eigenvector ϕ_i for molecular graphs ($i \in \{1, 2, 3\}$). Color indicates the value of each component (node) of the eigenvectors. (b) The architecture of Mol-PECO. Mol-PECO learns the positional encoding (LPE) with Transformer of graph Laplacian, and updates the atom embedding with GCN of Coulomb matrix and LPE. Specifically, GCN is implemented with skip-connection to relieve over-smoothing. Coulomb matrix, the fully connected graph representation, suppresses over-squashing with direct connections between nodes. With the updated atom embedding, Mol-PECO extracts the molecular embedding with sum pooling, and predicts 118 odor descriptors with neural networks of molecular embedding. In this work, p and d is set as 20 and 32, respectively.

We compare Mol-PECO with the baseline models (Table 2): the conventional GCN of graph representations, including the adjacency matrix and the CM, and the classifiers of fingerprint representations, including Mordreds features (mordreds)[Moriwaki et al., 2018], bit-based fingerprints (bfps)[Rogers and Hahn, 2010], and count-based fingerprints (cfps)[Rogers and Hahn, 2010]. Conventional classifiers include k -Nearest Neighbor (KNN), random forest (RF), and gradient boosting (GB). In the fingerprint methods, we first handle the problem of imbalanced label distribution with Synthetic Minority Over-sampling Technique (SMOTE)[Chawla et al., 2002], and then perform the classification. Mol-PECO outperforms the baselines in three out of six evaluation metrics (Table 2), with AUROC improved from 0.761 (cfps-KNN) to 0.813, AUPRC improved from 0.144 (mordreds-RF) to 0.181, and accuracy improved from 0.780 (Coulomb-GCN) to 0.808. Notably, Mol-PECO can balance AUROC (0.813) and AUPRC (0.181) whereas the ML method (cfps-KNN) with the highest AUROC of 0.761 has a low AUPRC of 0.057 and one (cfps-RF) with the highest AUPRC of 0.144 shows low AUROC of 0.723. Thus, Mol-PECO boosts the predictability of QSOR.

Table 2: Performance comparison of Mol-PECO with baseline methods, GCN, and Coulomb-GCN. The highest scores are shown in bold. The runner-ups are shown with underlines.

Baseline ¹	AUROC ²	AUPRC ²	Precision ²	Recall ²	Specificity ²	Accuracy ²
cfps-KNN	0.761	0.057	0.065	0.760	0.764	0.762
bfps-KNN	0.758	0.055	0.064	0.748	0.769	0.759
mordreds-KNN	0.729	0.052	0.062	0.676	0.783	0.730
mordreds-RF	0.723	0.144	<u>0.241</u>	0.483	0.964	0.723
cfps-RF	0.689	0.137	0.258	0.418	0.961	0.690
bfps-RF	0.671	0.119	0.227	0.381	<u>0.962</u>	0.672
mordreds-GB	0.725	0.126	0.220	0.499	<u>0.951</u>	0.725
cfps-GB	0.701	0.120	0.210	0.453	0.950	0.702
bfps-GB	0.687	0.111	0.193	0.428	0.948	0.688
adjacency-GCN	0.678	0.111	0.079	0.827	0.625	0.726
Coulomb-GCN	0.759	0.143	0.089	0.816	0.744	0.780
Mol-PECO-sym	<u>0.796</u>	<u>0.153</u>	0.088	0.817	0.787	<u>0.802</u>
Mol-PECO-asym	0.813	0.181	0.104	<u>0.819</u>	0.797	0.808

¹ Baseline includes conventional classifiers of fingerprint representations and graph convolutional networks (GCN) of molecular graphs. Fingerprint representations include count-based fingerprints (cfps), bit-based fingerprints (bfps), and Mordreds features (mordreds). The conventional classifiers include k -Nearest Neighbor (KNN), random forest (RF), and gradient boosting (GB). Molecular graph representations include adjacency matrix (adjacency-GCN) and Coulomb matrix (Coulomb-GCN). Mol-PECO-sym refers to the performances with LPE of raw Coulomb matrix. Mol-PECO-asym refers to the performances with LPE of asymmetrically normalized Coulomb matrix.

² The evaluation metrics are calculated in testing set.

3.3 Learned odor space by Mol-PECO

To investigate the learned structure of multiple odors in relation with descriptors, we perform dimensionality reduction over the output of Mol-PECO’s penultimate layer to build the latent odor space and evaluate it at global and local scales. At the global scale, we inspect how appropriately the clusters of odors in this latent space represent the information of descriptors, while, at the local scale, we examine whether individual molecules can possess a set of odor descriptors similar to those of nearby molecules or not.

For global structure, we analyze the distribution of the high-frequency descriptors, the structure-correlated descriptors, and the synonymy descriptors. For the high-frequency descriptors, we evaluate ‘odorless’, ‘fruity’, ‘green’, ‘woody’, ‘sweet’, and ‘floral’, which are the top six most assigned descriptors. The odorless molecules show a high AUROC value (AUROC = 0.94) and cluster far away from other molecules (Figure 5a, top left panel), verifying Mol-PECO’s ability to distinguish odorant and odorless molecules. Descriptor ‘woody’ localizes on the clusters at the middle of the odor space, whereas descriptors of ‘fruity’, ‘floral’, and ‘green’ are distributed across multiple clusters over the learned odor space (Figure 5a), indicating that ‘woody’ is a more different characteristic than ‘fruity’, ‘floral’, and ‘green’. As shown in Figure 2c, these three descriptors tend to co-occur. In the odor space, we can find clusters for different pairs of them, meaning that Mol-PECO can disentangle the differences between ‘fruity’-‘floral’, ‘floral’-‘green’, and ‘fruity’-‘green’. The descriptor ‘sweet’ achieves a low AUROC score (AUROC = 0.67) and the associated molecules spread over the space without a specific pattern, presumably reflecting its polysemous nature and strong association with taste.

For structure-correlated descriptors, molecules associated with ‘alliaceous’, ‘garlic’, or ‘onion’ appear in the cluster of ‘sulfurous’ compounds (Figure 5b) and show a very high score (AUROC = 0.97 – 0.98), in accordance with previous studies about sulfur compounds’ olfactory descriptions [Block, 1992, Miękus et al., 2020]. For synonymy descriptors, molecules of ‘oily’ and ‘fatty’ are clustered into neighbors, validating their similar semantics (Figure 5c).

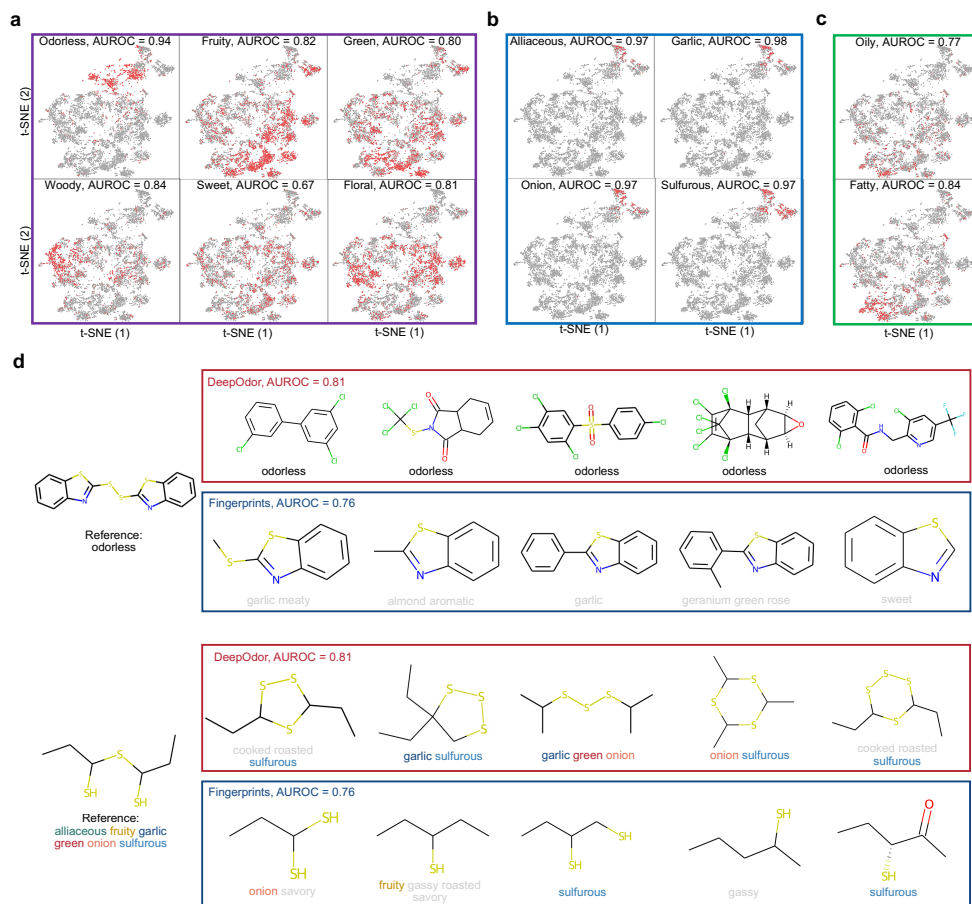


Figure 5: The odor space built from Mol-PECO and its global and local properties. Global view of the learned odor space with dimensionality reduction by t-SNE is shown in (a), (b), and (c) where each red or gray dot represents one odor molecule with and without the corresponding descriptor, respectively. The value of AUROC in each panel is the AUROC of the corresponding descriptor. (a) The descriptors with most molecules (‘odorless’, ‘fruity’, ‘green’, ‘woody’, ‘sweet’, and ‘floral’), (b) those for the sulfurous compounds (‘alliaceous’, ‘garlic’, and ‘onion’), and (c) those with similar semantic meaning (‘oily’ and ‘fatty’). (d) Local view of learned odor space investigated with nearest neighbor retrieval of reference odorless and odorant molecules. AUROC in (a), (b), and (c) refers to the AUROC of single odor descriptor. AUROC in (d) refers to the unweighted AUROC of 118 odor descriptors.

For local structure, we investigate one odorless molecule (triphenylphosphane) and one odorant molecule (1-(1-sulfanylpropylsulfanyl)propane-1-thiol with descriptors of ‘alliaceous’, ‘fruity’, ‘garlic’, ‘green’, ‘onion’, and ‘sulfurous’) as the examples (Figure 5d). We compare the top-5 nearest molecules searched by Mol-PECO’s embedding and bfps. The top-5 molecules of Mol-PECO and bfps are calculated with cosine similarity and Tanimoto similarity, respectively. For the odorless molecule, Mol-PECO retrieves all neighbors with the odorless descriptor, but bfps retrieves no molecule. Notably, the molecules fetched by Mol-PECO possess different substructures compared with the reference (e.g., all with C-Cl bond and top-2 / 3 / 5 with carbonyl functional group). For the odorant molecule, Mol-PECO retrieves all neighbors with shared descriptor, and bfps retrieves four. Moreover, all the molecules retrieved by bfps are open-chain structured, the same with the reference. In contrast, Mol-PECO retrieves quite different structured molecules, four of which are cyclic molecules. Both examples would indicate Mol-PECO’s promising potential in decoding molecules with different structures but identical smells.

4 Discussion

In this work, we develop Mol-PECO for predicting human olfactory perception from molecular structures. We handle this QSOR problem by improving the graph-neural-network-based approach from two aspects: the molecular representation and the graph modeling method. For molecular representation, we use CM, which is fully-connected and contains 3D conformer information (3D coordinates and charges of atoms), instead of adjacency matrix. For graph modeling, we use the positional encoding from the eigenfunctions of Laplacian to make up for GCN’s deficiency in directional modeling. Mol-PECO improves the olfactory perception prediction in two stages: starting from adjacency-GCN (AUROC of 0.678) to Coulomb-GCN (AUROC of 0.759) by introduction of CM, following by from Coulomb-GCN (AUROC of 0.759) to Mol-PECO with eigenfunctions of the symmetric (AUROC of 0.796) and asymmetric Laplacian (AUROC of 0.813).

These results indicate that improvement of the expressive power of GCN can greatly contribute to learning of non-trivial relationships between molecular structures and olfactory descriptors (labels) in the QSOR problem. Although extensions of NN architectures are typically accompanied by an increased cost of learning, the limited size of odorant molecules up to 400 daltons in molecular weight enables the practical application of such extended architectures. Thus, we believe that the QSOR problem provides a good real-world task to test and demonstrate the effectiveness of advanced architectures. In particular, pre-training of graph representation using unlabeled data may lead to further improvements in accuracy of QSOR prediction [Li et al., 2020, Hu et al., 2019]. In addition, as we found by experiments, employment of asymmetric Laplacians might also contribute to further technical advancements.

However, the QSOR problem suffers from ambiguity in the labels (descriptors) assigned to each molecule and also from low objectivity and consistency of the labeling conducted by few specialists [Trimmer et al., 2019, Keller et al., 2007]. In particular, individuals can have a quite different sense to highly ambiguous descriptors such as ‘sweet’ [Keller et al., 2007]. Thus, consistent labeling by individuals requires a certain amount of training, resulting in the difficulty to increase the amount of data. Moreover, for the prediction of mixed odors, which is important for applications, data acquisition is prohibitive due to the huge number of possible combinations [Meister, 2015]. In the future, it will be important to apply the approach developed in this paper to the prediction of more objective and systematically measurable outputs, such as the chemical properties of odorants [Pannunzi and Nowotny, 2019], the response of olfactory receptors [Bhandawat et al., 2005, Mainland et al., 2015], and the response of neural activity [Haddad et al., 2010, Lapid et al., 2011]. Such extensions will lead to more comprehensive and data-oriented understanding of chemical information coding in the olfactory system.

5 Materials and methods

5.1 Coulomb matrix and its normalization

As a molecular representation, Coulomb matrix is calculated mainly based on Coulomb repulsion force as follows:

$$C_{ij} = \begin{cases} 0.5Z_i^{2.4} & \text{for } i = j \\ \frac{Z_i Z_j}{|\mathbf{R}_i - \mathbf{R}_j|} & \text{for } i \neq j \end{cases}, \quad (1)$$

where C_{ij} refers to the entry in i^{th} row and j^{th} column, Z_i refers to the atomic charge, and R_i refers to the relative coordinates.

Considering the gap of minimal and maximal entries in Coulomb matrix, we perform 2 preprocessing methods to handle it, including matrix-wised Frobenius normalization and minmax normalization as follows:

$$\begin{aligned} \|C\|_F &= \sqrt{\sum_{i=1}^n \sum_{j=1}^n C_{ij}^2}, \\ C_{max} &= \max_{i,j} C_{ij}, \\ C_{min} &= \min_{i,j} C_{ij}, \end{aligned} \quad (2)$$

where $\|C\|_F$ refers to the normalization term of Frobenius normalization, C_{max} and C_{min} refer to the max and min term in minmax normalization. With the normalization term, we calculated the preprocessed Coulomb matrix as follows:

$$\begin{aligned} C^F &= C / (\|C\|_F + \epsilon), \\ C^M &= (C - C_{min}) / (C_{max} - C_{min} + \epsilon), \end{aligned} \quad (3)$$

where C^F and C^M refer to the Frobenius- and minmax- normalized matrix, and ϵ equals to 10^{-9} .

5.2 GCN of Coulomb matrix for multi-label classification

We build Coulomb-GCN based on Coulomb matrix with three modules: 1) atom embedding updating, 2) molecular embedding extraction, and 3) multi-label classification. In atom embedding updating, we use GCN with the residual mechanism to learn the molecular embedding as follows:

$$H^{(l)} = \sigma(XH^{(l-1)}W_{graph}^{(l-1)}) + H^{(l-1)}W_{linear}^{(l-1)}, \quad (4)$$

where $H^{(l)} \in R^{n \times d}$ refers to the updated atom embedding in l^{th} layer, $X \in R^{n \times n}$ refers to Coulomb matrix, $H^{(l-1)} \in R^{n \times h}$ refers to the updated atom embedding in $l-1^{\text{th}}$ layer, $W_{graph}^{(l-1)} \in R^{h \times d}$ refers to the parameters in GCN, $W_{linear}^{(l-1)} \in R^{h \times d}$ refers to the parameters in the linear transformation of $H^{(l-1)}$ for residual mechanism, $H^{(0)}$ refers to the random initialized atom embedding, n refers to the number of atom in molecule, d refers to the dimension of embedding in l^{th} layer, h refer to the dimension of embedding in $l-1^{\text{th}}$ layer, and σ refers to SELU activation function[Klambauer et al., 2017]. In molecular embedding extraction, we use the sum-pooling function as follows:

$$m_i = \sum_{j \in [n]} H_{ji}^{(l)}, \quad (5)$$

where m_i refers to the i^{th} entry in the molecular embedding of molecule m . In multi-label classification, we use fully-connected layers as follows:

$$y = \sigma(mW_{clf}), \quad (6)$$

where $m \in R^{1 \times d}$ refers to the learned molecular embedding, $W_{clf} \in R^{d \times o}$ refers to the parameters in the fully-connected layer, and o refers to the number of odor descriptors. Coulomb matrix and Coulomb-GCN have been implemented by Python (version 3.7.4) with deepchem (version 2.6.1) and pytorch (version 1.12.1).

5.3 Directional graph modeling by Laplacian for multi-label classification

Mol-PECO differs from Coulomb-GCN only in the atom embedding updating module, where we build the directional graph modeling with learned positional encoding (LPE).

The Laplacian matrix (L^1) of Coulomb matrix (X) is calculated as follows:

$$L^1 = D - X, \tag{7}$$

where D refers to the degree matrix. In LPE with eigen-decomposition of Laplacian, symmetrical Laplacian matrix is calculated for further spectral decomposition as follows:

$$\begin{aligned} L^2 &= I - D^{-1/2} X D^{-1/2} \\ &= D^{-1/2} D D^{-1/2} - D^{-1/2} X D^{-1/2} \\ &= D^{-1/2} (D - X) D^{-1/2} \\ &= D^{-1/2} L^1 D^{-1/2}. \end{aligned} \tag{8}$$

where I refers to the identity matrix. With the equations, L_2 is calculated with L_1 divided by $\sqrt{d_{ii}d_{jj}}$. Let $d_{ii} = \sum_{j=0}^{i-1} a_{ij} + \sum_{j=i+1}^n a_{ij} + a_{ii}$, then the Laplacian is calculated as follows:

$$\begin{aligned} L_{ij}^1 &= \sum_{j=0}^{i-1} a_{ij} + \sum_{j=i+1}^n a_{ij} + a_{ii} - a_{ii}, i = j, \\ L_{ij}^1 &= -a_{ij}, i \neq j, \end{aligned} \tag{9}$$

which indicates setting the diagonal entries zeros or not has no influence on L^1 and L^2 as $L^2 = D^{-1/2} L^1 D^{-1/2}$.

Minimization of quadratic form on graphs acts as the cost function of link/edge prediction and captures the global structural information. Naturally, the eigen-decomposition of Laplacian provides the solutions as follows:

$$f^* = \min_f f L^2 f^T = 1/2 \sum_{i,j} X(i,j) (f_i - f_j)^2, \tag{10}$$

where f^* refers to the eigenvectors of L . With Laplacian, Mol-PECO updates the positional encoding in an atom-wise manner proposed in Spectral Attention Network[Kreuzer et al., 2021]. Mol-PECO learns LPE in an atom-by-atom manner. Specifically, Mol-PECO first performs the linear transformation of eigenvalues and eigenvectors in a single atom, learns the positional information by Transformer, and then extracts the atom positional encoding by sum-pooling as follows:

$$\begin{aligned} W &= \Lambda W_0, \\ K &= Transformer(W), \\ e_i &= \sum_{j \in n} K_{ji}, \end{aligned} \tag{11}$$

where $\Lambda \in R^{p \times 2}$ refers to the p eigenvalues and eigenvectors for a single atom, $W_0 \in R^{2 \times d}$ refers to the parameters of the linear transformation in LPE, $K \in R^{p \times d}$ refers to the updated embedding with Transformer of $W \in R^{p \times d}$, and e_i refers to the i^{th} entry of single atom embedding (vector-shaped representation). Graph Laplacian and Mol-PECO have been implemented by Python (version 3.7.4) with deepchem (version 2.6.1) and PyTorch (version 1.12.1).

5.4 Loss functions

For both Coulomb-GCN and Mol-PECO, we build the classification loss with the binary cross-entropy loss function and a logarithm regularization term as follows:

$$\begin{aligned} l^i(y_{true}^i, y_{pred}^i) &= BCE(y_{true}^i, y_{pred}^i) + |\log(y_{pred}^i + \epsilon) - \log(y_{true}^i + \epsilon)|, \\ l(y_{true}, y_{pred}) &= \frac{1}{o} \sum_{i \in [o]} w_i l^i(y_{true}^i, y_{pred}^i), \end{aligned} \tag{12}$$

where y_{true}^i and y_{pred}^i refer to the ground truths and predictions of i^{th} odor descriptor, l^i refers to the loss function of i^{th} odor descriptor, BCE refers to the binary cross-entropy function, w_i refers to $1 - n_{pos}^i/n_{tot}$, n_{pos}^i refers to the number of positive samples in i^{th} descriptor, n_{tot} refers to the number of total samples. The training process has been implemented by Python (version 3.7.4) with PyTorch (version 1.12.1).

5.5 Molecular descriptors

We include three classical molecular descriptors in this work as the baseline molecular representations, including Mordred features (mordred)[Moriwaki et al., 2018], bit-based Morgan fingerprints (bfps)[Rogers and Hahn, 2010], and count-based Morgan fingerprints (cfps)[Rogers and Hahn, 2010]. Mordred calculates about 1825 features, including 214 2D and 1611 3D features. Both bfps and cfps encode the molecule’s topological environments (molecular fragments), which indicate the presence of atoms and functional groups, into a vector. Specifically, bfps encodes presence or absence of the molecular fragments as a binary information, while cfps encodes the number of atom/functional-group in the topological environment. The calculation of molecular descriptors has been implemented by Python (version 3.7.4) with mordred (version 1.2.0) and rdkit-pypi (version 2022.3.4).

5.6 Machine learning of molecular descriptors

Machine learning of molecular descriptors used in this work as baselines includes: 1) Synthetic Minority Over-sampling Technique (SMOTE)[Chawla et al., 2002] for handling the imbalanced label distribution, and 2) multiple binary classifiers for predicting multiple odor descriptors. For SMOTE, it performs minority sampling by generating new minority instances to expand the number of the minority class. For binary classifiers, we use K- Nearest Neighbor classifier (KNN), random forest classifier (RF), and gradient boosting classifier (GB). The KNN acts as a non-parametric classifier and predicts the label by voting from neighbors. RF acts as the ensemble learning of decision trees with sample bagging to decrease the variance of model and feature bagging to decrease the correlation among decision trees. GB builds multiple weak learners to minimize the differences between the true label and the predicted value by performing gradient decent. The procedures have been implemented by Python (version 3.7.4) with imblearn (version 0.9.0) and scikit-learn (version 1.0.2).

5.7 Acknowledgments

We thank the suggestions and discussion with all colleagues in laboratory for quantitative biology, IIS, Tokyo University and Takahiro G. Yamada, Yusuke Shibuya, and Mamoru Tomiyama in Funahashi-lab, Keio University. We also thank Yusuke Ihara and Chiori Ijichi for helpful comments. The work is supported by China Scholarship Council (CSC) Grant 202106230237 to M. Z., JSPS KAKENHI Grant Numbers 19H05799 to T.J.K., and JST CREST Grant Number JPMJCR2011 to A.F. and T.J.K.

References

- Noam Sobel, Vivek Prabhakaran, John E Desmond, Gary H Glover, RL Goode, Edith V Sullivan, and John DE Gabrieli. Sniffing and smelling: separate subsystems in the human olfactory cortex. *Nature*, 392(6673):282–286, 1998.
- Hadas Lapid, Sagit Shushan, Anton Plotkin, Hillary Voet, Yehudah Roth, Thomas Hummel, Elad Schneidman, and Noam Sobel. Neural activity at the human olfactory epithelium reflects olfactory perception. *Nature neuroscience*, 14(11):1455–1461, 2011.
- Charles S Sell. On the unpredictability of odor. *Angewandte Chemie International Edition*, 45(38): 6254–6261, 2006.
- Sanne Boesveldt, Mats J Olsson, and Johan N Lundström. Carbon chain length and the stimulus problem in olfaction. *Behavioural brain research*, 215(1):110–113, 2010.
- Andreas Keller, Richard C Gerkin, Yuanfang Guan, Amit Dhurandhar, Gabor Turu, Bence Szalai, Joel D Mainland, Yusuke Ihara, Chung Wen Yu, Russ Wolfinger, et al. Predicting human olfactory perception from chemical features of odor molecules. *Science*, 355(6327):820–826, 2017.

- Johannes Polster and Peter Schieberle. Structure–odor correlations in homologous series of mercaptoalkanols. Journal of Agricultural and Food Chemistry, 65(21):4329–4340, 2017.
- Lagnajit Pattanaik and Connor W Coley. Molecular representation: going long on fingerprints. Chem, 6(6):1204–1207, 2020.
- David Rogers and Mathew Hahn. Extended-connectivity fingerprints. Journal of chemical information and modeling, 50(5):742–754, 2010.
- Hiroto Moriawaki, Yu-Shi Tian, Norihito Kawashita, and Tatsuya Takagi. Mordred: a molecular descriptor calculator. Journal of cheminformatics, 10(1):1–14, 2018.
- Thomas N Kipf and Max Welling. Semi-supervised classification with graph convolutional networks. arXiv preprint arXiv:1609.02907, 2016.
- Albert Hofstetter, Lennard Bösel, and Sereina Riniker. Graph-convolutional neural networks for (qm) ml/mm molecular dynamics simulations. Physical Chemistry Chemical Physics, 24(37):22497–22512, 2022.
- Kevin Yang, Kyle Swanson, Wengong Jin, Connor Coley, Philipp Eiden, Hua Gao, Angel Guzman-Perez, Timothy Hopper, Brian Kelley, Miriam Mathea, et al. Analyzing learned molecular representations for property prediction. Journal of chemical information and modeling, 59(8):3370–3388, 2019.
- Evan N Feinberg, Debnil Sur, Zhenqin Wu, Brooke E Husic, Huanghao Mai, Yang Li, Saisai Sun, Jianyi Yang, Bharath Ramsundar, and Vijay S Pande. Potentialnet for molecular property prediction. ACS central science, 4(11):1520–1530, 2018.
- Xiaofeng Wang, Zhen Li, Mingjian Jiang, Shuang Wang, Shugang Zhang, and Zhiqiang Wei. Molecule property prediction based on spatial graph embedding. Journal of chemical information and modeling, 59(9):3817–3828, 2019.
- Michael Withnall, Edvard Lindelöf, Ola Engkvist, and Hongming Chen. Building attention and edge message passing neural networks for bioactivity and physical–chemical property prediction. Journal of cheminformatics, 12(1):1–18, 2020.
- Benjamin Sanchez-Lengeling, Jennifer N Wei, Brian K Lee, Richard C Gerkin, Alán Aspuru-Guzik, and Alexander B Wiltschko. Machine learning for scent: Learning generalizable perceptual representations of small molecules. arXiv preprint arXiv:1910.10685, 2019.
- Devin Kreuzer, Dominique Beaini, Will Hamilton, Vincent Létourneau, and Prudencio Tossou. Rethinking graph transformers with spectral attention. Advances in Neural Information Processing Systems, 34:21618–21629, 2021.
- Kenta Oono and Taiji Suzuki. Graph neural networks exponentially lose expressive power for node classification. arXiv preprint arXiv:1905.10947, 2019.
- Jake Topping, Francesco Di Giovanni, Benjamin Paul Chamberlain, Xiaowen Dong, and Michael M Bronstein. Understanding over-squashing and bottlenecks on graphs via curvature. arXiv preprint arXiv:2111.14522, 2021.
- Wely B Floriano, Nagarajan Vaidehi, William A Goddard III, Michael S Singer, and Gordon M Shepherd. Molecular mechanisms underlying differential odor responses of a mouse olfactory receptor. Proceedings of the National Academy of Sciences, 97(20):10712–10716, 2000.
- Matthias Rupp, Alexandre Tkatchenko, Klaus-Robert Müller, and O Anatole Von Lilienfeld. Fast and accurate modeling of molecular atomization energies with machine learning. Physical review letters, 108(5):058301, 2012.
- Vijay Prakash Dwivedi and Xavier Bresson. A generalization of transformer networks to graphs. arXiv preprint arXiv:2012.09699, 2020.
- Dominique Beaini, Saro Passaro, Vincent Létourneau, Will Hamilton, Gabriele Corso, and Pietro Liò. Directional graph networks. In International Conference on Machine Learning, pages 748–758. PMLR, 2021.

- Steffen Arctander et al. Perfume and flavor materials of natural origin. Perfume and Flavor Materials of Natural Origin, 1960.
- Yogesh Kumar, Om Prakash, Himanshu Tripathi, Sudeep Tandon, Madan M Gupta, Laiq-Ur Rahman, Raj K Lal, Manoj Semwal, Mahendra Pandurang Darokar, and Feroz Khan. Aromadb: A database of medicinal and aromatic plant's aroma molecules with phytochemistry and therapeutic potentials. Frontiers in plant science, 9:1081, 2018.
- Neelansh Garg, Apuroop Sethupathy, Rudraksh Tuwani, Rakhi Nk, Shubham Dokania, Arvind Iyer, Ayushi Gupta, Shubhra Agrawal, Navjot Singh, Shubham Shukla, et al. Flavordb: a database of flavor molecules. Nucleic acids research, 46(D1):D1210–D1216, 2018.
- T Acree. Flavornet and human odor space. <http://www.flavornet.org/flavornet.html>, 2004.
- Fragrance Flavor. Food, and cosmetics ingredients information. the good scents company.
- International Fragrance Association et al. Gc/ms quantitation of potential fragrance allergens in fragrance compounds, 2003.
- John C Leffingwell. Olfaction ii. Leffingwell reports, 1(4):1–26, 2001.
- Anju Sharma, Rajnish Kumar, Shabnam Ranjta, and Pritish Kumar Varadwaj. Smiles to smell: decoding the structure–odor relationship of chemical compounds using the deep neural network approach. Journal of Chemical Information and Modeling, 61(2):676–688, 2021.
- Anju Sharma, Bishal Kumar Saha, Rajnish Kumar, and Pritish Kumar Varadwaj. Olfactionbase: a repository to explore odors, odorants, olfactory receptors and odorant–receptor interactions. Nucleic Acids Research, 50(D1):D678–D686, 2022.
- Sigma-Aldrich Corporation. Aldrich Chemistry 2012-2014: Handbook of Fine Chemicals. Sigma-Aldrich, 2011.
- Piotr Szymański and Tomasz Kajdanowicz. A network perspective on stratification of multi-label data. In First International Workshop on Learning with Imbalanced Domains: Theory and Applications, pages 22–35. PMLR, 2017.
- Joshua Schrier. Can one hear the shape of a molecule (from its coulomb matrix eigenvalues)? Journal of Chemical Information and Modeling, 60(8):3804–3811, 2020.
- Omar Mahmood, Elman Mansimov, Richard Bonneau, and Kyunghyun Cho. Masked graph modeling for molecule generation. Nature communications, 12(1):1–12, 2021.
- Yuyang Wang, Jianren Wang, Zhonglin Cao, and Amir Barati Farimani. Molecular contrastive learning of representations via graph neural networks. Nature Machine Intelligence, 4(3):279–287, 2022.
- Bojan Mohar, Y Alavi, G Chartrand, and OR Oellermann. The laplacian spectrum of graphs. Graph theory, combinatorics, and applications, 2(871-898):12, 1991.
- Fan RK Chung. Spectral graph theory, volume 92. American Mathematical Soc., 1997.
- Daniel Spielman. Spectral graph theory. Combinatorial scientific computing, 18, 2012.
- Nitish V Chawla, Kevin W Bowyer, Lawrence O Hall, and W Philip Kegelmeyer. Smote: synthetic minority over-sampling technique. Journal of artificial intelligence research, 16:321–357, 2002.
- Eric Block. The organosulfur chemistry of the genus allium—implications for the organic chemistry of sulfur. Angewandte Chemie International Edition in English, 31(9):1135–1178, 1992.
- Natalia Miękus, Krystian Marszałek, Magdalena Podlacha, Aamir Iqbal, Czesław Puchalski, and Artur H Świergiel. Health benefits of plant-derived sulfur compounds, glucosinolates, and organosulfur compounds. Molecules, 25(17):3804, 2020.
- Pengyong Li, Jun Wang, Yixuan Qiao, Hao Chen, Yihuan Yu, Xiaojun Yao, Peng Gao, Guotong Xie, and Sen Song. Learn molecular representations from large-scale unlabeled molecules for drug discovery. CoRR, abs/2012.11175, 2020. URL <https://arxiv.org/abs/2012.11175>.

- Weihua Hu, Bowen Liu, Joseph Gomes, Marinka Zitnik, Percy Liang, Vijay S. Pande, and Jure Leskovec. Pre-training graph neural networks. *CoRR*, abs/1905.12265, 2019. URL <http://arxiv.org/abs/1905.12265>.
- Casey Trimmer, Andreas Keller, Nicolle R Murphy, Lindsey L Snyder, Jason R Willer, Maira H Nagai, Nicholas Katsanis, Leslie B Vosshall, Hiroaki Matsunami, and Joel D Mainland. Genetic variation across the human olfactory receptor repertoire alters odor perception. *Proceedings of the National Academy of Sciences*, 116(19):9475–9480, 2019.
- Andreas Keller, Hanyi Zhuang, Qiuyi Chi, Leslie B Vosshall, and Hiroaki Matsunami. Genetic variation in a human odorant receptor alters odour perception. *Nature*, 449(7161):468–472, 2007.
- Markus Meister. On the dimensionality of odor space. *Elife*, 4:e07865, 2015.
- Mario Pannunzi and Thomas Nowotny. Odor stimuli: not just chemical identity. *Frontiers in physiology*, 10:1428, 2019.
- Vikas Bhandawat, Johannes Reiser, and King-Wai Yau. Elementary response of olfactory receptor neurons to odorants. *Science*, 308(5730):1931–1934, 2005.
- Joel D Mainland, Yun R Li, Ting Zhou, Wen Ling L Liu, and Hiroaki Matsunami. Human olfactory receptor responses to odorants. *Scientific data*, 2(1):1–9, 2015.
- Rafi Haddad, Tali Weiss, Rehan Khan, Boaz Nadler, Nathalie Mandairon, Moustafa Bensafi, Elad Schneidman, and Noam Sobel. Global features of neural activity in the olfactory system form a parallel code that predicts olfactory behavior and perception. *Journal of Neuroscience*, 30(27):9017–9026, 2010.
- Günter Klambauer, Thomas Unterthiner, Andreas Mayr, and Sepp Hochreiter. Self-normalizing neural networks. *CoRR*, abs/1706.02515, 2017. URL <http://arxiv.org/abs/1706.02515>.

A Appendix

A.1 Parameter tuning of Mol-PECO

We optimize Mol-PECO with different number of Transformer layers in learned positional encoding and choose 4 as the optimized parameter (Table 3).

Table 3: Scores of Mol-PECO with different number of Transformer layers and the layer number optimization. The highest scores are shown in bold.

#Transformer layers	AUROC ¹	AUPRC ¹	Precision ¹	Recall ¹	Specificity ¹	Accuracy ¹
1	0.809	0.170	0.103	0.826	0.789	0.807
2	0.798	0.147	0.100	0.817	0.779	0.798
3	0.807	0.163	0.090	0.831	0.779	0.805
4	0.813	0.181	0.104	0.819	0.797	0.808
5	0.807	0.181	0.089	0.819	0.780	0.800
6	0.802	0.162	0.093	0.814	0.790	0.802

¹ The evaluation metrics are calculated with the validation set.

The training process of the optimized parameter (the number of Transformer layer = 4) is monitored by the loss curves (Figure 6a). The decreased trends of the loss curves are consistent, indicating that Mol-PECO has found the right bias/variance tradeoff in the training and validation sets. Mol-PECO chooses the checkpoint of 554 epochs with minimal loss of 0.140 as the final model for testing (Figure 6b).

After training and validation, we obtain the detailed performances of 118 odor descriptors in 6 evaluation metrics (Figure 7).

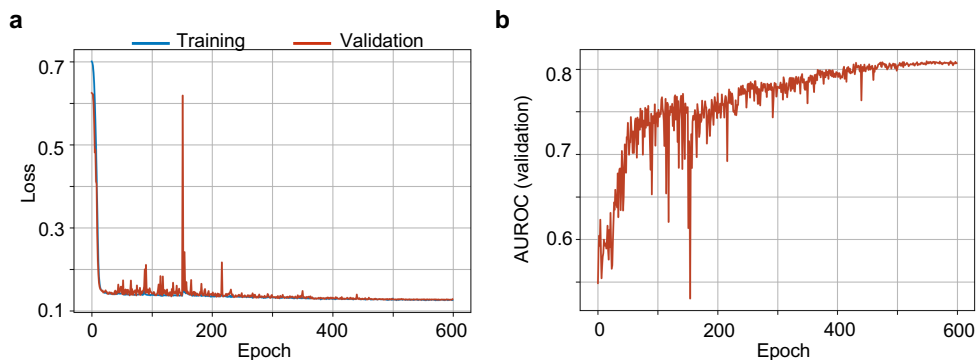


Figure 6: The training process with the optimized parameter. (a) The unweighted loss during training. (b) The unweighted AUROC during training.

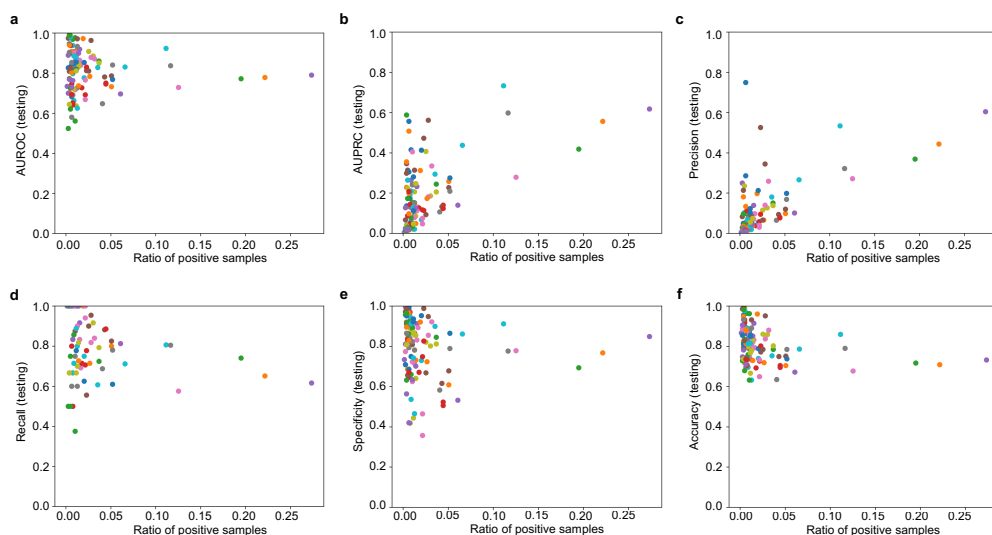


Figure 7: The detailed performances of Mol-PECO in 6 evaluation metrics, including (a) AUROC, (b) AUPRC, (c) Precision, (d) Recall, (e) Specificity, and (f) accuracy. The x-axis refers to the ratio of positive samples. Each dot refers to one odor descriptor.

A.2 Supplementary materials for the learned odor space

Despite of the high-frequency descriptors, the structure-correlated descriptors, and the synonymy descriptors, we also investigate the alcohol-related descriptors, the fruit-related descriptors, and the synonym descriptors in Figure 8. For alcohol-related descriptors, ‘ethereal’ and ‘winery’ possess the most molecules, leading to an obvious cluster in nearby locations (Figure 8a). For the fruit-related descriptors, ‘apple’, ‘banana’, ‘pear’, and ‘pineapple’ are clustered together (Figure 8b). For synonymy descriptors, partial ‘roasted’ and full ‘cooked’ are clustered into neighbors, validating their similar semantics (Figure 8c).

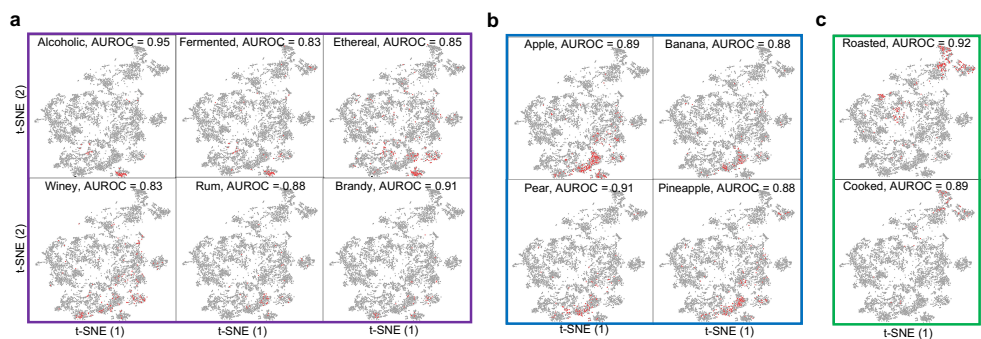


Figure 8: Global view of learned odor space with dimensionality reduction by t-SNE in (a) the alcohol-related descriptors ('alcoholic', 'fermented', 'ethereal', 'winey', 'rum', and 'brandy'), (b) the fruit-related descriptors ('apple', 'banana', 'pear', and 'pineapple'), and (c) the molecules with similar semantic meaning ('roasted' and 'cooked').